P14.2 LIGHTNING AND RADAR OBSERVATIONS OF TWO STORMS OBSERVED DURING STEPS

Sarah A. Tessendorf*, Kyle C. Wiens, and Steven A. Rutledge
Colorado State University, Fort Collins, Colorado

1. INTRODUCTION

The Severe Thunderstorm Electrification and Precipitation Study (STEPS; Lang et al. 2004) field campaign took place between 17 May 2000 and 20 July 2000 in eastern Colorado and western Kansas. STEPS research aims to identify relationships between microphysics, dynamics and electrification in severe storms on the High Plains, and in particular, investigate positive cloud-to-ground (CG) lightning production. One specific scientific goal of STEPS, as outlined in the Scientific Overview[1], is "To understand the formation of precipitation and its influence on electrical development, especially in those storms producing large hail." This study focuses on that specific goal by contrasting kinematic, microphysical, and electrical characteristics of two STEPS cases: a positive CG-producing storm and a storm that produced no CG flashes.

On 29 June 2000, a positive CG-producing severe thunderstorm propagated through the STEPS multiple-Doppler radar network between 2130 UTC[2] (29 June) and 0115 (30 June). It produced large hail and an F1 tornado, in addition to copious lightning. To date, this storm has received much attention by the STEPS community and several studies discuss the characteristics of this storm in detail (MacGorman et al. 2004, Tessendorf et al. 2004, Wiens et al. 2004). On 3 June 2000, an isolated cell was observed in the far northeastern extent of the STEPS radar network between 2210 (3 June) and 0121 (4 June). It produced three-quarter inch hail and frequent intra-cloud (IC) lightning, but no CGs of either polarity. This study provides a preliminary discussion of the 3 June storm and compares the relationships among the kinematic, microphysical, and electrical properties that characterize the 3 June and 29 June storms.

* *Corresponding author address:* Sarah A. Tessendorf, Colorado State Univ., Dept. of Atmospheric Science, Fort Collins, CO 80523-1371; e-mail: saraht@atmos.colostate.edu

[1] http://www.mmm.ucar.edu/pdas/steps-science.html

[2] All times hereafter are listed in UTC.

2. DATA AND METHODS

Instrumentation and observing systems operated during STEPS that are most central to this study included three S-Band Doppler radars (two of which were polarimetric research radars) for mapping the three-dimensional structure of precipitation and storm winds, the National Lightning Detection Network (NLDN), and a 3-D lightning mapping network operated by New Mexico Institute of Mining and Technology.

2.1 Radar data and processing

The CSU-CHILL polarimetric Doppler radar, the National Center for Atmospheric Research (NCAR) S-Pol polarimetric Doppler radar, and the Goodland, Kansas National Weather Service (NWS) WSR-88D radar comprised the triple-Doppler radar network used to take the radar measurements. The three radars were arranged in a rough equilateral triangle with approximately 60-km sides (Figure 1).

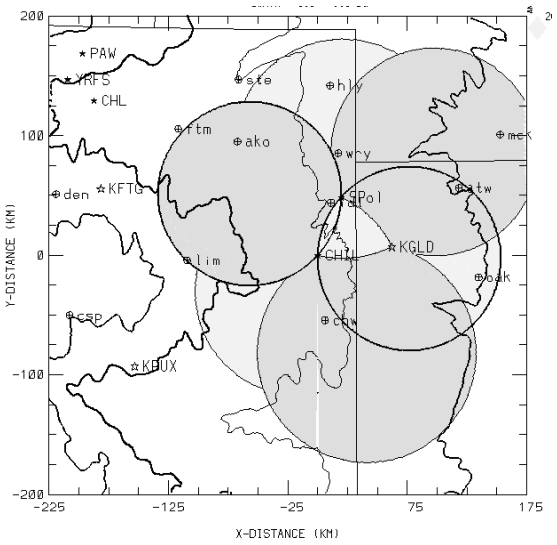

Figure 1. The STEPS research domain: radar locations and dual-Doppler lobes (shaded) are displayed.

All three radars are S-band Doppler radars; however, the CSU-CHILL and NCAR S-Pol radars are dual linearly polarized. This capability enables the radar to detect hydrometeor shape and size

that, when combined with air temperature, can be used to infer hydrometeor type.

Wind field syntheses were completed for 25 volume scans during the period 2301 (3 June)-0121 (4 June)[3] and for 37 volume scans during the period 2130 (29 June)-0115 (30 June). The radar data were interpolated onto a Cartesian grid using NCAR's Sorted Position Radar INTerpolator (SPRINT). Grid resolution was 0.5 km in both the horizontal and vertical directions. After the grid interpolation, the velocity data were globally unfolded by means of NCAR's Custom Editing and Display of Reduced Information in Cartesian Space (CEDRIC) software (Mohr et al. 1986). The three dimensional wind fields were computed using the radial velocities from all three radars when available; otherwise winds were computed from only two radars. The speed and direction of storm movement were calculated for each case and used for the advection parameters. The vertical velocities were obtained using a variational integration of the continuity equation (O'Brien 1970).

The polarimetric data were edited to eliminate noise, clutter, and suspect data following the methods outlined in Ryzhkov and Zrnic (1998). The processed data were then gridded in the same manner as described above. For the 3 June case, polarimetric data was available from either CHILL or S-Pol between 2210 (3 June) and 0121 (4 June). A fuzzy-logic hydrometeor classification scheme, (hereafter FHC), adapted from Liu and Chandrasekar (2000) and Straka et al. (2000), was implemented for the Cartesian gridded data to estimate bulk hydrometeor types within the storm (Tessendorf et al. 2004). Hydrometeor echo volumes were also calculated for each radar scan time by multiplying the number of grid points (N) that satisfied the FHC category of interest by the volume of a grid box (0.125 km^3). The polarimetric results and the vertical motion estimates were then compared versus time for the analysis periods.

2.2 Lightning data and processing

The New Mexico Tech Lightning Mapping Array (LMA; Rison et al. 1999) provides measurements of the time and three-dimensional location of very high frequency (VHF) radiation sources emitted by lightning discharges. For a given lightning flash, the LMA may locate hundreds to thousands of such sources resulting in detailed maps of the total lightning activity.

To determine total (CG plus IC) flash rates, we used an algorithm developed at New Mexico Tech (Thomas et al. 2003) which sorts the LMA sources into discrete flashes. To infer charge structure, we analyzed the LMA data on a flash-by-flash basis using the bi-directional discharge model (Kasemir 1960; Mazur and Ruhnke 1993) as the basis for interpretation. For example, we assumed that flashes initiate in strong electric field between regions of opposite net charge and propagate bi-directionally into the charge regions on either side. The negative breakdown component of a lightning flash is noisier at VHF, and thus more often detected by the LMA compared to the positive breakdown component. Assuming that negative (positive) breakdown traverses regions of net positive (negative) charge, we infer the qualitative structure of the charge regions involved in the flash based on the temporal evolution of the flash and on the relative number of LMA sources on either side of the flash initiation location. Most IC flashes reveal distinct vertically-separated "layers" of charge, with many more LMA sources in the inferred positive layer.

3. OBSERVATIONS FROM 3 JUNE 2000

3.1 Overview

The environment on 3 June 2000 was characterized by strong south-southwesterly surface winds between 15-20 kts (gusts to near 25 kts) in front of a surface boundary. The winds were slightly weaker and northwesterly behind the boundary. Surface temperatures ahead of the boundary were near 90° F, and dew points were in the mid-50s° F. Behind the boundary the temperatures were similar, yet the dew points were in the mid-30s° F. The surface boundary was likely a dry line that was moving in conjunction with a trough line. The upper-level winds were westerly near 50 kts (Fig. 2). In the 0012 MGLASS sounding, the CAPE was a marginal value of 700 J kg^{-1} (Fig. 2). Notable drying was evident above 500 mb as well.

[3] The S-Pol radar went down for 20 minutes prior to the 0026 volume scan and therefore syntheses could not be performed during that period.

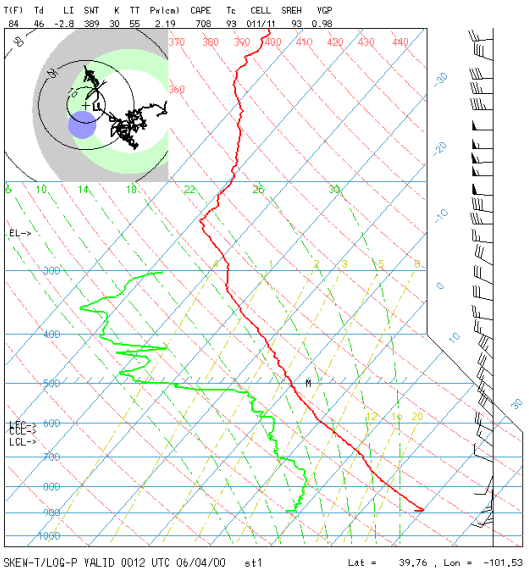

Figure 2. MGLASS sounding at 0012 UTC on 4 June 2000 near Bird City, KS.

Near 1700, the surface boundary appeared as a convergence line in the radial velocity field and as a weak thin line echo in radar reflectivity. The boundary was oriented from southwest to northeast, and propagated southeastward. Near 2230, two small cells (labeled A and B in Fig. 3) developed in southwestern Nebraska along the northern end of this boundary. Intra-cloud lightning was first detected near 2240. By 2330, cell B merged into the forward left flank of cell A. A visible split in the upper level radar reflectivity echo was observed at 2356, and the left-moving cell diminished soon thereafter. By 0030 the maximum updraft had declined to near 5 m s^{-1} and after that the radar reflectivity echo continued to get smaller over time until the storm had completely dissipated by 0121.

3.2 Time series

The temporal evolution of the maximum updraft in the 3 June storm began[4] near 20 m s^{-1} and reached a maximum of ~25 m s^{-1} near 2350 (Fig. 4). By 0026, peak updrafts were near 13 m s^{-1} and soon thereafter declined to 5 m s^{-1} and steadily decreased beyond that. Graupel was first detected by the FHC algorithm near 2235 in the mid-levels of the storm and steadily increased in echo volume until near 2320, at which time graupel amounts leveled off until near 2350 (Figs. 4, 5). After this time, the graupel echo volume attained its maximum value of near 1000 km^3 at 0002, most of which was centered near 7 km MSL[5] (Fig. 4). Total hail echo volume was minimal and detected only between 2320 and 0026 near 3 km, except between 0000 and 0010 where a small amount of hail echo was identified near 8 km (Fig. 4). One other point to note is that total hail echo volume is comprised of the FHC small hail and large hail categories, and, for this storm, large hail was scarcely detected.

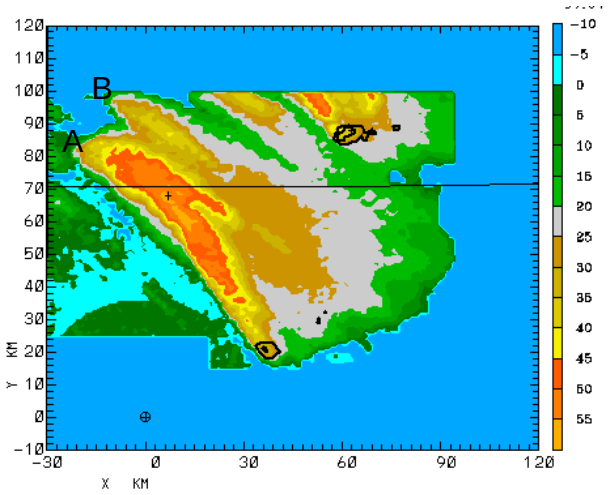

Figure 3. Swath of maximum in the vertical column KGLD reflectivity (dBZ) for the period 2236-0121 UTC. Radar locations are denoted with a '⊕' symbol, with KGLD at (x,y)=(0,0).

These trends in graupel and hail echo volumes seemed to lag the trend in updraft volume greater than 10 m s^{-1} (hereafter, UV10). Shortly after the first synthesis time, UV10 rose sharply and then peaked just prior to 2320, which was just before the first peak in graupel echo volume and the initial detection of hail echo volume (Fig. 5). By 2331, UV10 began to rise sharply again, and then peaked its maximum value at 2344. The all-time maximum in graupel echo volume happened within 15 minutes of this UV10 peak.

The relationship between lightning and graupel echo in this storm reinforces the importance of active riming growth in the electrification process. There was no lightning

[4] Due to the less than desirable location of the storm relative to the dual-Doppler domain, synthesis could not be performed until after the storm had already developed and therefore the maximum updraft at first measurement was already near 20 m s^{-1}.

[5] All heights hereafter will be in kilometers above mean sea level (MSL).

until graupel was detected, and the trend in total lightning flash rate closely followed that of graupel echo volume (Fig. 5). The maximum flash rate in this storm was near 36 flashes per minute and occurred at 0002 when the graupel echo volume reached its peak.

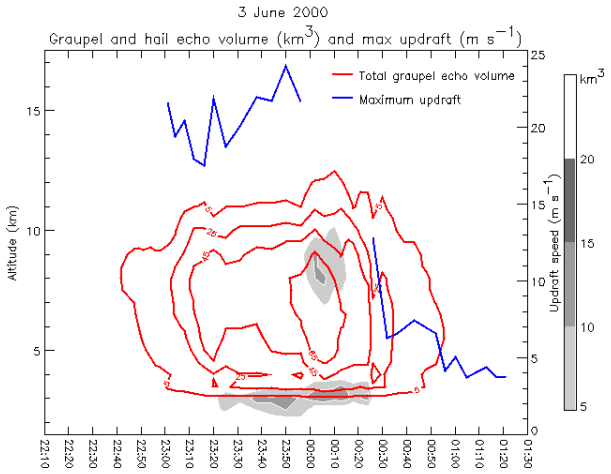

Figure 4. Time-height cross-sections of total graupel echo volume and total hail echo volume (gray shaded contours), and maximum updraft time series (values on right axis) for 3 June 2000.

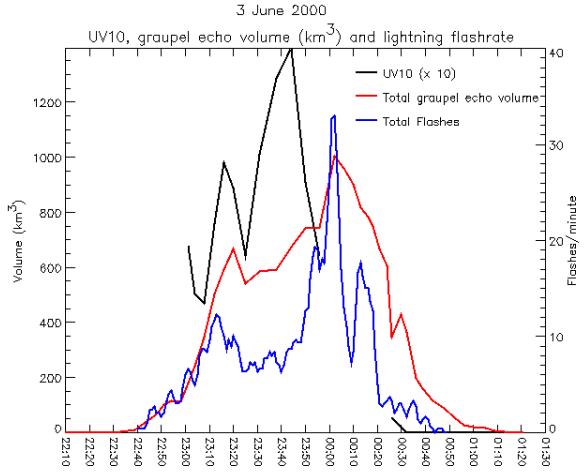

Figure 5. Time series of updraft volume greater than 10 m s^{-1} (multiplied by 10 to fit on left axis), total graupel echo volume (values on left axis), and the counted flash rate from the LMA data (values on right axis) for 3 June 2000.

3.3 Charge structure

Throughout the duration of the 3 June storm, the vast majority of lightning flashes occurred near the precipitation core of the storm and initiated downward from 9-11 km altitude with relatively dense LMA sources below the flash origin and relatively sparse LMA sources above. This describes what could be termed an inverted dipole, with a negative charge region near 10-12 km altitude (T<-40°C) and positive charge below. Some such "inverted" IC flashes remained vertically compact in the upper part of the storm, with the positive charge centered near 10km (T≈-30°C) within strong (>30dBZ) lofted echo. However, most of the inverted flashes extended much further, with the positive charge sloping downward east of the updraft, apparently following the descent of the precipitation. Hence, the lower positive charge may have consisted of multiple layers or simply one deep region. There were never any flashes that indicated an intervening negative charge region within the lower positive charge. As the time-height contours of total LMA sources in Fig 6 indicate, the bulk of the LMA sources were constrained between 5-10 km altitude, which is the same altitude range that we consistently identified as the positive charge region of an inverted dipole in our flash-by-flash analysis.

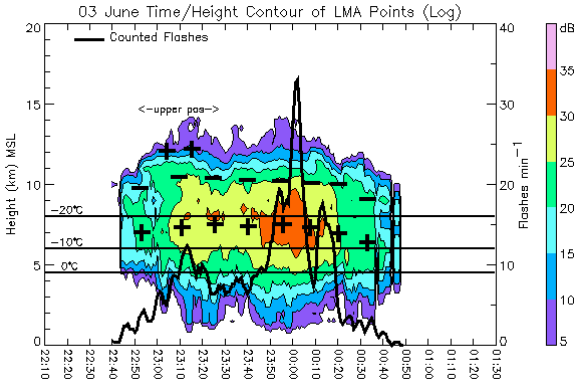

Figure 6. Time height contours of total LMA sources (color-shaded in logarithmic units) with total flash rate time series for 3 June 2000. Plus and minus symbols indicate gross LMA-inferred charge structure.

Assuming charge-separating collisions are primarily responsible for thunderstorm electrification, the implication of this observed charge structure is that larger ice particles (e.g., graupel) received positive charge in rebounding

collisions, while smaller ice particles (e.g., ice crystals) received negative charge. Whether or not this is consistent with laboratory charging studies (i.e. Takahashi 1978, Saunders et al. 1991) that base the sign of charge transferred on temperature and cloud liquid water content will be explored in future work.

In addition to the persistent presence of this inverted dipole, there was a roughly 30 minute time-span (2255-2325) during which several flashes initiated upward from 10-12 km into an inferred upper positive charge region that lay near the upper radar echo boundary of the storm. Flashes involving the upper positive charge were generally within the anvil, further downwind (east) of the core, and these upper flashes migrated further from the core with time. To illustrate this charge structure, Fig.7 shows four representative flashes overlaid onto radar cross-sections near 2325. The flash in the eastern anvil in Fig.7 was the last clear flash that involved the upper positive charge.

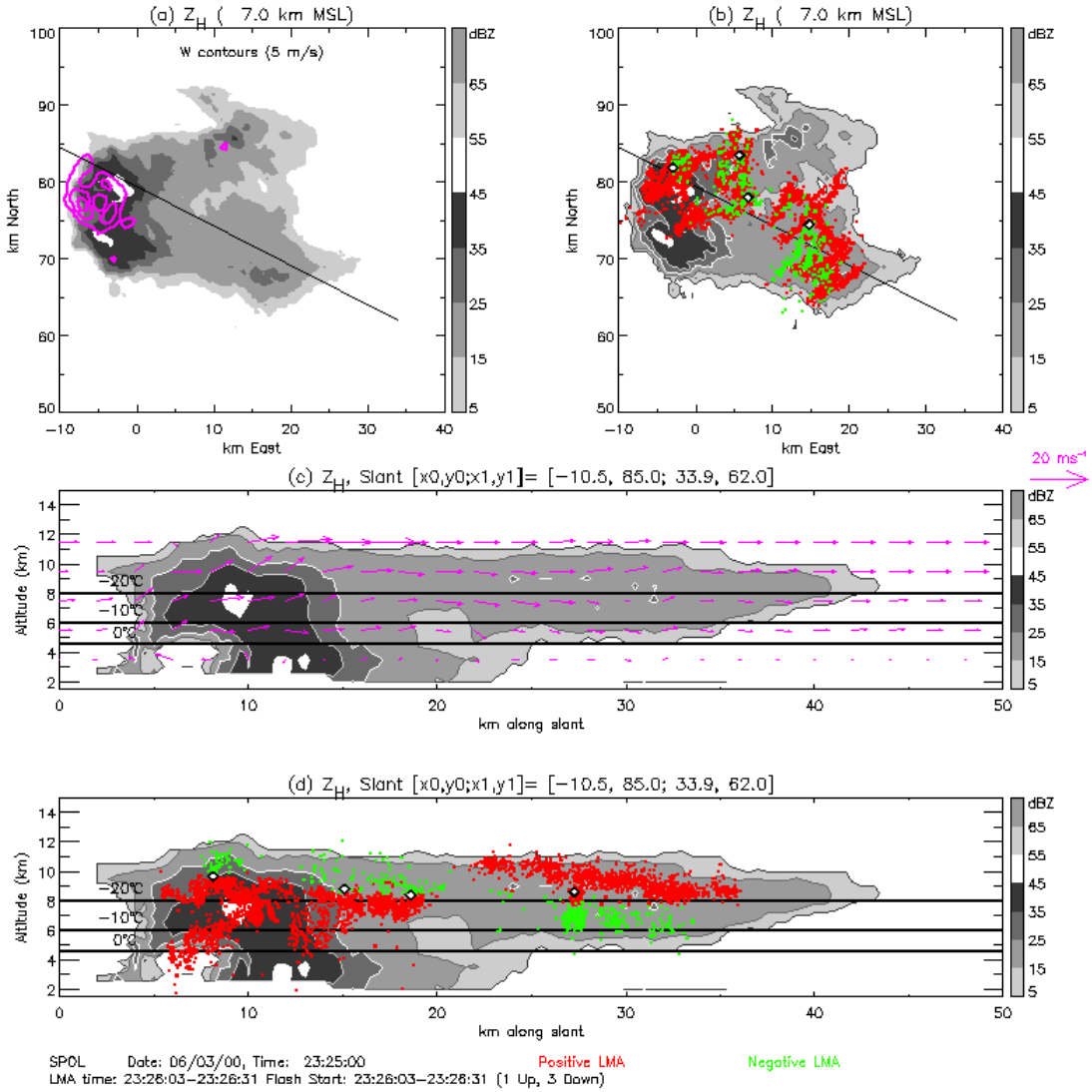

Figure 7. Cross-sections of radar reflectivity (gray-shaded) and Doppler-derived winds during volume scan beginning at 2325 on 3 June 2000. Magenta contours in (a) show Doppler-derived updraft in 5 m s^{-1} intervals. LMA sources from four representative flashes are overlaid onto (b) and (d) and color-coded according to inferred charge region, with red for positive and green for negative. Filled diamond symbols indicate the first LMA sources in each flash.

4. COMPARISON WITH 29 JUNE 2000

On 29 June 2000, upper level winds were stronger than those on 3 June 2000 (Fig. 8). Surface conditions between the two cases were quite similar; both storms formed along a southeastward propagating surface boundary near Bird City, Kansas, with similar surface temperatures and dew point contrasts across the boundary. However, Convective Available Potential Energy (CAPE) was higher on 29 June (measured at 1254 J kg^{-1} by the 2022 MGLASS sounding, Fig. 8) and a mid-level shortwave that passed over the area that day may have also enhanced storm dynamics.

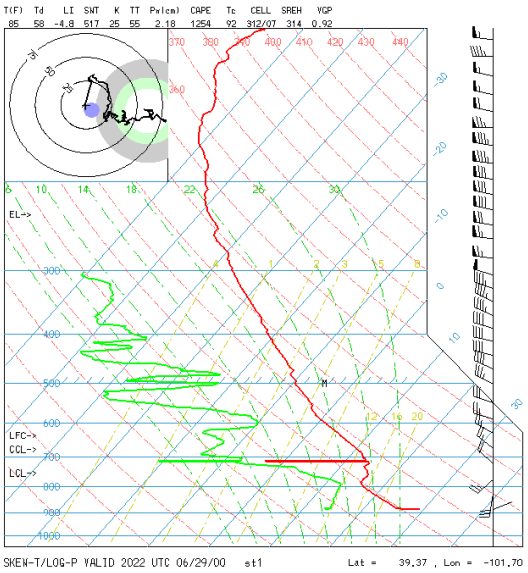

Figure 8. MGLASS sounding at 2022 UTC on 29 June 2000 near Goodland, KS.

The early evolution of the 29 June storm was similar to that of the 3 June storm; both storms developed along the surface boundary and exhibited multiple (weak) updraft cores. Prior to 2230, the 29 June storm had similar maximum updraft speeds, UV10, graupel echo volume, and lightning flash rates (Figs. 4, 5, 9, 10). Contrary to this early period in 29 June, the 3 June storm did not exhibit hail echo volume aloft (Figs. 4, 9). Beyond 2230, the 29 June storm intensified into a much stronger storm than 3 June, kinematically (updraft strength), microphysically (echo volumes of graupel and hail), and electrically (lightning flash rates, both IC and CG). Maximum updraft speeds were twice as strong as those of 3 June (up to 50 m s^{-1}), and much larger quantities of hail and graupel echo volumes, in addition to UV10, were observed (Figs. 9, 10). Moreover, the 29 June storm developed strong cyclonic vorticity on its right flank past 2230, whereas cyclonic vorticity in 3 June was much weaker, and short-lived (not shown).

The lack of large hail in the 3 June storm could be attributed to a few factors: primarily a deficiency of hail embryos in and near the low-level updraft, and the lack of a strong updraft to sustain growth of large particles, particularly, too little volume of updraft greater than 10 m s^{-1} (approximate updraft speed required to sustain growth of hail greater than 2 cm). The reduced CAPE on 3 June, compared to 29 June, might be one possible explanation for its weaker kinematic intensity. The deficiency of embryos might have also resulted from the absence of cyclonic vorticity on the right flank of the storm. In the 29 June storm, cyclonic vorticity was shown to be an important factor in hail growth as it recirculated mm-sized particles (which descended from the upper-level stagnation zone) into the main low-level updraft for further growth into hail (Tessendorf et al 2004). It is also possible that the liquid water content available in the mixed phase region of the 3 June storm was not sufficient for large hail growth, but this has not been determined at this point.

The lightning flash rates on 29 June were on the order of 100s per minute, in contrast to 10s per minute in 3 June (Figs. 5, 10). The 29 June storm began producing +CG lightning during periods of rapid hail growth and overall storm intensification, while the 3 June storm never produced a single CG flash of either polarity, according to the NLDN observations. Why did the 3 June storm not produce any CGs? In terms of LMA-inferred charge structure, both the 3 June and 29 June storms were dominated by inverted IC flashes between an upper-negative and a deep mid-to-low-level positive charge region, but the 29 June storm was much more electrically complex and active (Fig 11). In particular, the 29 June storm developed alternating lower-level charge regions outside the updraft. As described in Wiens et al. (2004), the 29 June storm produced many upward initiating flashes from a lower negative charge region that lay below and downwind of the deep positive. The 29 June storm began producing +CGs after the manifestation of this lower negative charge, and most of the +CGs initiated and struck ground near it. In contrast, the 3 June storm

showed no evidence of a lower negative charge region. Perhaps this lower negative region may be the impetus required for the deep positive charge to deliver its charge to ground in the form of +CGs.

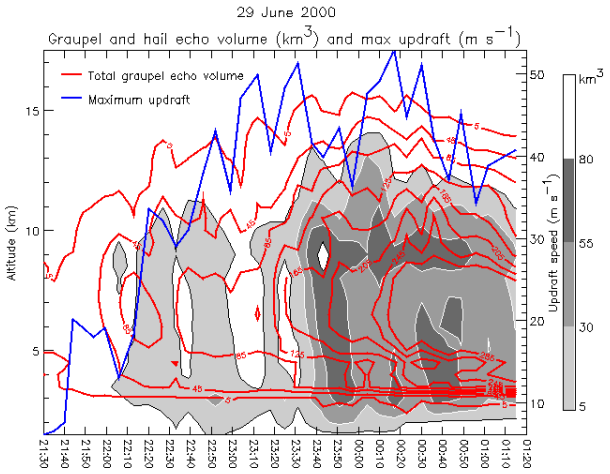

Figure 9. Same as Figure 4 except for 29 June 2000.

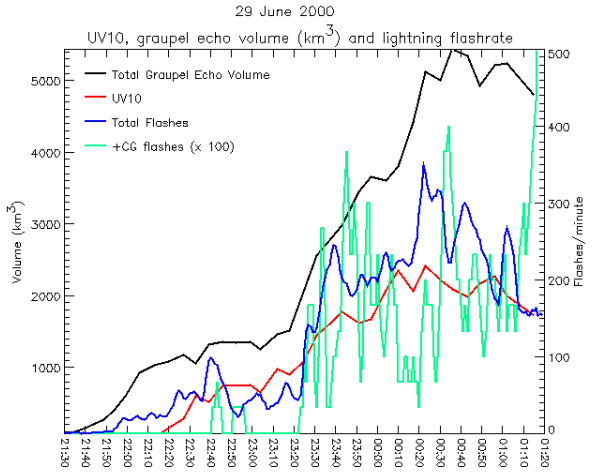

Figure 10. Same as Figure 5 except with positive CG flash rate trend and for 29 June 2000.

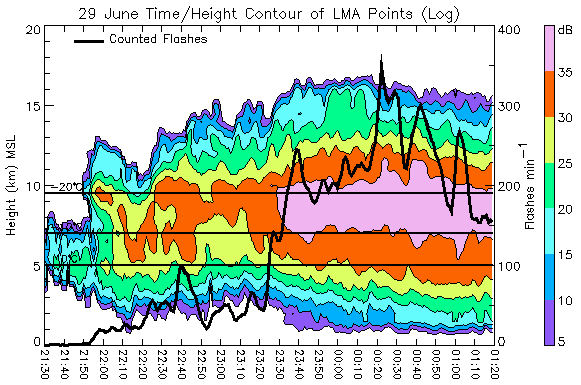

Figure 11. Time height contours of total LMA sources (color-shaded in logarithmic units) with total flash rate time series for 29 June 2000.

5. CONCLUDING REMARKS

The objective of this project was to examine relationships among the kinematic, microphysical, and electrical aspects of the 3 June supercell in comparison with those of the 29 June supercell. Radar data from the CSU-CHILL, NCAR S-Pol, and Goodland WSR-88D radars were synthesized to determine the three dimensional wind fields, and polarimetric variables from the CSU-CHILL and NCAR S-Pol radars were used to estimate the bulk hydrometeor types within the storms. LMA data were analyzed to determine lightning flash rates and charge structure within the storms.

In summary, the 3 June storm was different from the 29 June storm in that it had weaker updrafts, smaller ice contents (graupel and hail), and lower lightning flash rates. Both storms exhibited an inverted dipole charge structure, yet the 29 June storm produced CG flashes, which were mostly of positive polarity, while the 3 June storm did not produce any CGs of either polarity. This preliminary analysis has invoked numerous questions about the processes that lead to hail and positive CG lightning. Such questions that we will continue to investigate are:

1) Why didn't the 3 June storm produce large hail, and as much hail as 29 June?
2) Why did both storms have an inverted dipole charge structure?
3) Why didn't 3 June exhibit a lower negative charge layer while 29 June did?
4) What role, if any, does hail have in the charging process and does it relate to the

generation of the lower negative charge layer?

5) What other microphysical processes might lead to the lower negative charge layer?

Future work will include an analysis of a negative CG-producing storm on 19 June 2000 for comparison with the two cases discussed herein. A more detailed examination of the 3 June storm for each radar volume scan will be done, as well as an analysis of the liquid water content profile and potential for the storm to produce hail via a simple particle growth model.

Acknowledgements: We would like to thank L. Jay Miller of NCAR for support with the multiple-Doppler analysis. Thanks to Dr. Larry Carey (Texas A&M) for assistance with the polarimetric data processing and hydrometeor identification algorithm suggestions. The S-Pol and KGLD radar data were obtained from NCAR. We thank Dr. Paul Krehbiel, Dr. William Rison, Dr. Ron Thomas, Tim Hamlin, and Jeremiah Harlin of New Mexico Tech for the LMA data and software. This research was supported by the National Science Foundation Physical Meteorology Program under grant ATM-0118021.

REFERENCES

Kasemir, H. W., 1960: A contribution to the electrostatic theory of lightning discharge. *J. Geophys. Res*., **65**, 1873-1878.

Lang, T.J., and co-authors, 2004: The severe thunderstorm electrification and precipitation study. *Bull. Amer. Meteor. Soc,* in press.

Liu, H., and V. Chandrasekar, 2000: Classification of hydrometeors based on polarimetric radar measurements: Development of fuzzy logic and nuero-fuzzy systems and in situ verification. *J. Atmos. Oceanic Technol.*, **17**, 140-164.

MacGorman, D.R., W.D. Rust, P. Krehbiel, E. Bruning, and K. Wiens, 2004: The electrical structure of two supercell storms during STEPS. *Mon. Wea. Rev*., in review.

Mazur, V. and L. H. Ruhnke, 1993: Common physical processes in natural and artificially triggered lightning. *J. Geophys. Res*., **98**, 12,913-12,930.

Mohr, C.G., L.J. Miller, R.L. Vaughn, and H.W. Frank, 1986: On the merger of mesoscale data sets into a common Cartesian format for efficient and systematic analysis. *J. Atmos. Oceanic. Technol.*, **3**, 143-161.

O'Brien, J.J., 1970: Alternative solutions to the classical vertical velocity problem. *J. Appl. Meteor.*, **9**, 197-203.

Rison, W., R. J. Thomas, P. R. Krehbiel, T. Hamlin, and J. Harlin, 1999: A GPS-based three-dimensional lightning mapping system: Initial observations in Central New Mexico. *Geophys. Res. Lett*., **26**, 3573-3576.

Ryzhkov, A.V. and D.S. Zrnic, 1998: Polarimetric rainfall estimation in the presence of anomalous propagation. *J. Atmos. Oceanic Technol.*, **15**, 1320-1330.

Saunders, C. P. R., W. D. Keith, and R. P. Mitzeva, 1991: The effect of liquid water on thunderstorm charging. *J. Geophys. Res*., **96**, 11,007-11,017.

Straka, J.M., D.S. Zrnic, and A.V. Ryzhkov, 2000: Bulk hydrometeor classification and quantification using polarimetric radar data: Synthesis of relations. *J. Appl. Meteor.*, **39**, 1341-1372.

Takahashi, T., 1978: Riming electrification as a charge generation mechanism in thunderstorms. *J. Atmos. Sci.,* **35**, 1536-1548.

Tessendorf, S.A., L.J. Miller, K.C. Wiens, and S.A. Rutledge, 2004: The 29 June 2000 supercell observed during STEPS. Part I: Kinematics and microphysics. *J. Atmos. Sci.,* in review.

Thomas, R., P. Krehbiel, W. Rison, J. Harlin, T. Hamlin, and N. Campbell, 2003: The LMA flash algorithm. Abstract C4-23, *Proc. 12th Intl. Conf. On Atmos. Elect*., 655-656, Versailles, France.

Wiens, K.C., S.A. Rutledge, and S.A Tessendorf, 2004: The 29 June 2000 supercell observed during STEPS. Part II: Lightning and charge structure. *J. Atmos. Sci.,* in review.